Dynamic Mechanical Loading Enhances the Regenerative Potency of Meniscus Cell-Derived Extracellular Vesicles

Catherine Cheung[1], Zizhao Li[1], Sung-Han Jo[1], Se-Hwan Lee[1], Jina Ko[1], Su Chin Heo[1]
[1]University of Pennsylvania, Philadelphia, PA 19104
catwxy@seas.upenn.edu

DISCLOSURES: Catherine Cheung (N), Zizhao Li (N), Sung-Han Jo (N), Se-Hwan Lee (N), Jina Ko (N), Su Chin Heo (5-4WEB Medical)

INTRODUCTION: The meniscus provides essential support to healthy knee function by facilitating joint mobility, stability, and lubrication [**1**], but its high injury prevalence results in approximately 850,000 surgeries annually in the United States [**2**]. Due to the tissue's limited intrinsic healing capacity, nearly two-thirds of patients with meniscus tears develop osteoarthritis within 15 years [**3**], highlighting the need for therapeutics to enhance endogenous meniscus healing. Extracellular vesicles (EVs), nanoscale mediators of intercellular communication, have recently emerged as promising biological therapeutics capable of modulating inflammation and enhancing matrix regeneration [**4**]. Our prior work demonstrated that cyclic dynamic tensile loading of outer zone meniscus fibrochondrocytes (MFCs) significantly increased EV production compared to static conditions [**5**]. Furthermore, EVs derived from loaded MFCs ("mechanically primed EVs") induced stable and increased expressions of type I collagen and aggrecan, respectively, in mesenchymal stromal cells (MSCs), suggesting loading-dependent enhancement of their regenerative potency [**5**]. However, the mechanosensitive mechanisms governing MFC-derived EV biogenesis and the corresponding changes in EV surface and cargo compositions remain unknown. We *hypothesized* that dynamic loading increases the yield of EVs through a mechanosensitive pathway and enriches their cargo with regenerative cues promoting meniscus repair.

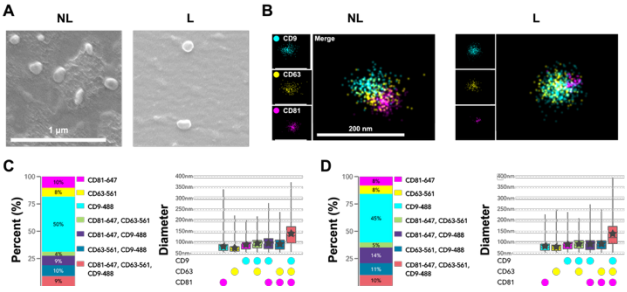

Fig 1: (A-B) Representative **(A)** SEM and **(B)** STORM images of NL-EVs (left) and L-EVs (right). **(C–D)** Quantitative distributions of the canonical surface tetraspanins CD9, CD63, and CD81 (left) and corresponding EV diameter histograms (right) for **(C)** NL-EVs (n = 2,144 EVs) and **(D)** L-EVs (n = 2,326 EVs).

METHODS: Outer zone MFCs were seeded onto aligned polycaprolactone (PCL) scaffolds and pre-cultured for 2 days before undergoing either free-swelling culture (NL-EVs) or cyclic dynamic loading (L-EVs) in a custom bioreactor as previously described [**5**]. Mechanical loading was applied at 3% strain amplitude and 1 Hz frequency for 3 hours. EVs were isolated via ultracentrifugation of the conditioned medium [**6**]. For morphological characterization, EVs were sputter-coated with iridium and imaged using a FEI Quanta FEG 250 scanning electron microscope (SEM). Super-resolution microscopy (STORM) images were acquired using the ONI EV Profiler Kit 2 following manufacturer protocols, and images were analyzed using AutoEV and CODI (ONI). For pharmacological inhibition of various mechanotransduction pathways, Y27632 (10 µM), verteporfin (1 µM), BAPTA-AM (25 µM), or GW4869 (20 µM) were added to culture medium prior to loading. Nanoparticle tracking analysis (NTA) was used to quantify EVs [**5**]. For proteomics samples, MFC-laden PCL scaffolds were subjected to daily loading (3% strain, 1 Hz, 1 hour/day) for three consecutive days (3dL-EVs), and EVs were collected via PEG precipitation [**7**]. SDS-PAGE confirmed protein enrichment and liquid chromatography-tandem mass spectrometry (LC-MS/MS) was used to identify and quantify EV protein cargo.

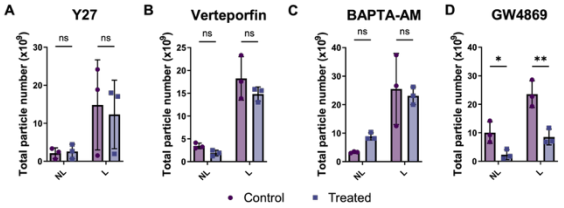

Fig 2: Total number of particles detected by NTA following treatment with **(A)** Y27632, **(B)** Verteporfin, **(C)** BAPTA-AM, and **(D)** GW4859 (n=3 donors each).

RESULTS: SEM images of both non-loading (NL) and mechanically primed (L) samples showed several particles smaller than 200 nm with circular morphologies consistent with typical EVs (**Fig 1A**). STORM imaging of the canonical tetraspanins, CD9, CD63, and CD81, followed by clustering analysis, revealed comparable surface expression and size distributions between NL-EVs and L-EVs (**Fig 1B-D**). Pharmacological inhibition of RhoA/ROCK (Y27632, **Fig 2A**), YAP/TAZ (verteporfin, **Fig 2B**), or Ca^{2+} signaling (BAPTA-AM, **Fig 2C**) did not significantly alter EV yield under either non-loading or mechanical loading conditions. In contrast, inhibition of the ESCRT-independent EV biogenesis pathway (GW4869) significantly decreased EV release in both groups (**Fig 2D**). SDS-PAGE analysis confirmed robust protein enrichment in EV isolates, with both NL-EV and 3dL-EV samples showing more diverse protein bands compared to their corresponding cell-free media controls (**Fig 3A**). After filtering out media-derived proteins, LC-MS/MS identified 380 total proteins, of which 48 (12.6%) were unique to NL-EVs, 153 (40.3%) were unique to 3dL-EVs, and 179 (47.1%) were shared between both groups (**Fig 3B**). Protein-protein interaction analysis revealed strong connectivity among proteins upregulated in 3dL-EVs (**Fig 3C**). Gene ontology (GO) enrichment analysis of the top 30 upregulated proteins revealed biological process terms associated with extracellular matrix modeling and tissue development, and molecular function terms related to glycosaminoglycan binding (**Fig 3D**).

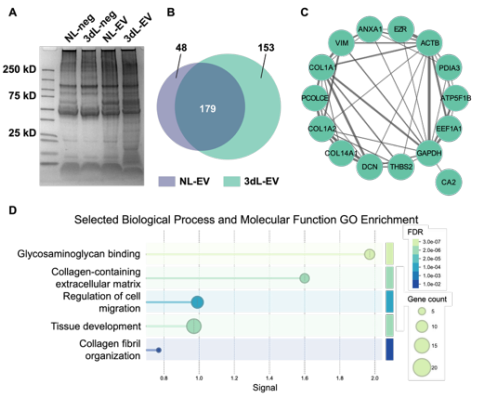

Fig 3: (A) SDS-PAGE of NL-EV and 3dL-EV proteins compared to cell-free controls. **(B)** Venn diagram of proteins found in EVs **(C)** Protein network of top proteins upregulated in 3dL-EVs vs. NL-EVs. **(D)** GO enrichment of top proteins upregulated in 3dL-EVs compared to NL-EVs, selected terms.

DISCUSSION: This study extensively characterized EVs derived from MFCs under static and dynamic loading conditions. While dynamic loading significantly increased EV yield, their morphology and surface tetraspanin profiles remained consistent, suggesting conserved biophysical integrity. Pharmacological inhibition studies revealed that EV biogenesis/secretion do not strongly depend on classical mechanotransduction pathways such as RhoA/ROCK, YAP/TAZ, and intracellular calcium signaling. Instead, disruption of the ceramide-mediated, ESCRT-independent pathway markedly reduced EV output, suggesting its involvement in mechanically regulated EV release. Proteomic profiling demonstrated that mechanical loading enriched EV cargo with proteins associated with extracellular matrix organization, cell migration, tissue development, and glycosaminoglycan binding, which collectively suggests enhanced regenerative potential. Together, these findings indicate that dynamic mechanical loading augments both the yield and bioactivity of MFC-derived EVs through mechanosensitive and ceramide-dependent processes. Confirmation of these results *in vivo* will be needed to further validate the therapeutic efficacy of these mechanically primed EVs. This work identifies mechanical priming as a scalable strategy to generate functionally potent EVs for meniscus repair and broader musculoskeletal tissue regeneration.

SIGNIFICANCE: This study provides further evidence supporting the therapeutic use of mechanically primed MFC-derived EVs for meniscus injury treatment, as dynamic loading amplifies both the yield of EVs and their regenerative capacity. This approach offers a scalable and clinically translatable method for generating bioactive EV formulations to promote meniscus healing and prevent post-injury degeneration.

REFERENCES: [1] Fox+ 2015, Clin. Anat., [2] Luvsannyam+ 2022, Cureus, [3] Riera+ 2011, Arthritis Res. Ther., [4] Magdy+ 2020, Appl. Sci. 10, [5] Cheung+ ORS 2025, [6] Théry+ 2006, Curr. Protoc. Cell Biol., [7] Weng+ 2016, Analyst.

ACKNOWLEDGEMENTS: This work was supported by the NIH (R01 AR079224, R01 HL163168, P50 AR080581) and NSF (CMMI-1578571).